Computational and Structural Biotechnology Journal 21 (2023) 5174–5185

Contents lists available at ScienceDirect

Computational and Structural Biotechnology Journal

journal homepage: www.elsevier.com/locate/csbj

Research article

HELLS modulates the stemness of intrahepatic cholangiocarcinoma through promoting senescence-associated secretory phenotype

Xiaojing Du [a,b,c,1], Xingxing Zhang [d,e,1], Zhuoran Qi [a,b,f,1], Ziyi Zeng [g,1], Ye Xu [a,b], Zhijie Yu [d,h,*,2], Xin Cao [a,i,**,3], Jinglin Xia [a,b,d,**,4]

[a] Zhongshan Hospital, Fudan University, Shanghai 200032, China
[b] Liver Cancer Institute, Zhongshan Hospital, Fudan University, Shanghai 200032, China
[c] Endoscopy Center, Shanghai East Hospital, Tongji University School of Medicine, Shanghai, China
[d] Key Laboratory of Diagnosis and Treatment of Severe Hepato-Pancreatic Diseases of Zhejiang Province, The First Affiliated Hospital of Wenzhou Medical University, Wenzhou 325000, China
[e] Department of Gastroenterology, Shanghai University of Medicine & Health Sciences Affiliated Sixth People's Hospital South Campus, Shanghai 201499, China
[f] Department of Gastroenterology, Zhongshan Hospital, Fudan University, Shanghai 200032, China
[g] Royal Prince Alfred Hospital, 50 Missenden Rd, Camperdown, NSW 2050, Australia
[h] Wenzhou Key Laboratory of Hematology, The First Affiliated Hospital of Wenzhou Medical University, Wenzhou 325000, China
[i] Institute of Clinical Science, Zhongshan Hospital, Fudan University, Shanghai 200032, China

ARTICLE INFO

Keywords:
Intrahepatic cholangiocarcinoma
Cancer stem like cells
HELLS
Cell senescence
Senescence-associated secretory phenotype

ABSTRACT

The senescence-associated secretory phenotype (SASP) is closely associated with the tumorigenesis and progression of intrahepatic cholangiocarcinoma (ICC). However, it remains unclear its relation to stemness of ICC. In the study, the stemness indices of ICC were calculated using one-class linear regression (OCLR) and single-sample gene set enrichment analysis (ssGSEA) algorithms. A total of 14 senescence-related stemness genes (SRSGs) were identified using Pearson correlation analysis in ICC. Subsequently, a SRSGs-related classification was established using a consensus clustering for ICC. Different types of ICC exhibit distinct prognosis, immunity, metabolisms, and oncogenic signatures. Additionally, we constructed a risk score model for ICC using principal component analysis (PCA). The risk score was positively correlated with stemness, immune infiltration, metabolisms and oncogenic signatures, but negatively with prognosis in ICC. Patients with a high risk score may respond well to immunotherapy. Furthermore, we employed 3D fibrin gels to select tumor-repopulating cells (TRC) with stemness features. We found that HELLS, belonging to the 14 SRSGs, was up-regulated in ICC-TRC. And silencing HELLS significantly reduced the colony size, inhibited migration and invasion, and attenuated SASP in ICC-TRC. In summary, we provided a novel classification and risk score for ICC and uncovered a molecular mechanism *via* which CSLCs could obtain an active SASP.

Abbreviations: SASP, senescence-associated secretory phenotype; ICC, intrahepatic cholangiocarcinoma; OCLR, one class linear regression; ssGSEA, single sample gene set enrichment analysis; SRSGs, senescence-related stemness genes; PCA, principal component analysis; TRC, tumor-repopulating cells; CSLCs, cancer stem like cells; Helicase, lymphoid specific, HELLS; mOS, median overall survival; EMT, epithelial-to-mesenchymal transition; SRGs, senescence-related genes; HAGR, Human Ageing Genomic Resources; TCGA, the Cancer Genome Atlas; GEO, Gene Expression Omnibus; SS, senescence score; RNA-seq, RNA-sequencing; TPM, transcripts per kilobase million; mRNAsi, mRNA expression-based stemness index; NTP, nearest template prediction; TME, tumor microenviroment; TIDE, tumor immune dysfunction and exclusion; TIP, tumor immune phenotype; MSigDB, Molecular Signatures Database; GSVA, gene set variation analysis; GSEA, gene set enrichment analysis; DEGs, differentially expressed genes; qRT-PCR, quantitative reverse transcription polymerase chain reaction; PVDF, polyvinylidene difluoride; SA-β-Gal, senescence-associated β-galactosidase; RFS, relapse-free survival; PCC, Pearson correlation coefficient; BP, biological process; MF, molecular function; CC, cellular component.

* Corresponding author at: Key Laboratory of Diagnosis and Treatment of Severe Hepato-Pancreatic Diseases of Zhejiang Province, The First Affiliated Hospital of Wenzhou Medical University, Wenzhou 325000, China.
** Corresponding authors at: Zhongshan Hospital, Fudan University, Shanghai 200032, China.
E-mail addresses: zhijie_yu@wzhospital.cn (Z. Yu), caox@fudan.edu.cn (X. Cao), xia.jinglin@zs-hospital.sh.cn (J. Xia).
[1] Xiaojing Du, Xingxing Zhang, Zhuoran Qi and Ziyi Zeng contribute equally to this work.
[2] ORCID: 0000-0003-3442-4066
[3] ORCID: 0000-0003-1722-023X
[4] ORCID: 0000-0003-1566-3934

https://doi.org/10.1016/j.csbj.2023.09.020
Received 11 May 2023; Received in revised form 17 September 2023; Accepted 17 September 2023
Available online 7 October 2023

1. Introduction

Intrahepatic cholangiocarcinoma (ICC), originating from the bile ducts above the second order, ranks the second most common primary liver cancer, accounting for up to 20% of all hepatic malignancies [1]. Its incidence has increased more than 140% over the past 4 decades, with an increase from 0.44 to 1.18 cases per 100,000 people between 1973 and 2012 in USA [1]. Unfortunately, so many patients are diagnosed at an advanced stage that miss the chance of surgical resection. The median overall survival (mOS) for patients treated with the current standard-of-care chemotherapy regimen (gemcitabine and cisplatin) is less than one year [1,2], indicating the poor prognosis. Recent advances in researchers' knowledge of ICC have resulted in the implementation of targeted therapy for about 40% of patients, including those in fibroblast growth factor receptor (FGFR) and isocitrate dehydrogenase (IDH), but resistance comes within months of initiation [1]. These factors lead to ICC a subject of intense research.

Cancer stem like cells (CSLCs) are a small subset of tumor cells, which are tumorigenic, metastatic, resistant to chemotherapy and radiotherapy, and, they also contribute to tumor recurrence [3]. These cell subpopulations with stem cell characteristics played a crucial role in oncogenesis, progression, metastasis, recurrence, as well treatment resistance in ICC. Targeted therapies to eradicate CSLCs may assist in overcoming treatment resistance and reduce the rates of relapse and recurrence in ICC [3]. Cell senescence is a typically irreversible form of proliferative arrest, which is mediated by intricate mechanisms, including genomic instability, epigenetic alterations, chronic inflammation, dysbiosis, chromatin remodeling, DNA damage *etc.* [4]. It evokes alterations in cell morphology and metabolism and, most profoundly, a senescence-associated secretory phenotype (SASP) involving the release of excessive bioactive factors (such as chemokines, interleukins, and proteases) [4]. With increasing evidence, it is clear that SASP affects multiple processes including cell proliferation, epithelial-to-mesenchymal transition (EMT), angiogenesis, therapy resistance and immunosuppression, *etc.* in a broad range of cancer types [5,6]. Recently, association between cell senescence and stemness has attracted a great attentions. Cell senescence can transform non-stem bulk leukaemia cells into self-renewing, leukaemia-initiating stem cells [7]. SASP also favors the stemness of multiple myeloma and hepatocellular carcinoma [8,9]. However, little is know about relation between cell senescence and CSLCs in ICC, and therefore insights into it may bring out a potential therapy strategy for ICC.

To investigate the role of cell senescence in ICC, senescence-related genes (SRGs) were downloaded from Human Ageing Genomic Resources (HAGR) database [10], and ICC data from the Cancer Genome Atlas (TCGA) as well Gene Expression Omnibus (GEO). Senescence-related stemness genes (SRSGs) were identified by one class linear regression (OCLR) and single sample gene set enrichment analysis (ssGSEA) algorithms in ICC [11,12]. Moreover, SRSGs were used to cluster ICC *via* an unsupervised clustering and its correlation to the clinic, molecular, metabolism and immunity of ICC was also evaluated. In addition, a SRSGs based senescence score (SS) with prognosis signature has been established in ICC. Finally, as a representative SRSGs, we found that HELLS may promote stemness of ICC *via* activating SASP.

2. Methods and materials

2.1. Source of RNA-sequencing and microarray data

RNA-sequencing (RNA-seq) data of human ICC CHOL and GSE107943 were downloaded from TCGA and GEO, respectively [13,14]. Microarray data were from GEO, including GSE32879, GSE76311 (TIGER-LC), GSE107102, GSE89749 (Table S1) [15–18]. For the RNA-seq data, raw counts were transformed into transcripts per kilobase million (TPM) values. The quality control of all microarray datasets has been conducted and showed in Fig. S1. Corresponding clinical data were downloaded from TCGA and GEO databases and showed in Table S2.

2.2. Calculation of stemness indices

Stemness indices were determined using ssGSEA and OCLR algorithms aiming at investigating stemness feature of ICC samples [11,12]. The ssGSEA algorithm was frequently used to calculate the enrichment score of certain gene set, which indicated the enrichment level of this signature in the sample [12]. Accordingly, the stemness genes were obtained from Miranda's studies and applied to ssGSEA algorithm to calculate ssGSEA-based stemness index (Table S3 and S4) [19]. OCLR is another machine learning that utilizes transcriptome data to evaluate stemness features [11]. OCLR calculated stemness index was termed as mRNA expression-based stemness index (mRNAsi), being achieved using a "synapser" package (http://ran.synapse.org/) of R (version 4.2.0; Table S4).

2.3. Identification of ICC subclasses

To identify SRSGs in ICC, SRGs were downloaded from HAGR [10] (n = 307, Table S5). SRSGs were recognized using the Pearson correlation analysis between the expression of SRGs and ssGSEA-based stemness index or mRNAsi in ICC samples. Based on the genes, a SRSGs-related classification was established by using a consensus clustering [20]. In addition, previous classifications of ICC were predicated by using nearest template prediction (NTP) analyses based on the provided subclass specific signatures, being achieved by GenePattern website (https://cloud.genepattern.org/) [14,18,21–23].

2.4. Estimation of cancer immunity

The tumor microenviroment (TME) score was determined by using ESTIMATE and xCELL algorithms to evaluated TME characteristics of ICC [24,25]. Several algorithms were used to estimate the cell infiltration in TME of ICC, including CIBERSORT, Epic, MCPcounter, Quantiseq, ssGSEA and xCELL [12,24–28]. Tumor immune dysfunction and exclusion (TIDE) algorithm was achieved by using TIDE website [29]. Cancer immunity cycle consisted of seven steps, 1) release of cancer cell antigens, 2) cancer antigen presentation, 3) priming and activation, 4) trafficking of T cells to tumors, 5) infiltration of T cells into tumors, 6) recognition of cancer cells by T cells, and 7) killing of cancer cells. The related gene sets were obtained from the tracking tumor immune phenotype (TIP) [30] website and quantified by using the ssGSEA algorithm.

2.5. Enrichment analysis

To conduct function enrichment analysis, c2.cp.kegg.v7.4.symbols and h.all.v7.5.1.symbols were obtained from the Molecular Signatures Database (MSigDB) [31]. Gene set variation analysis (GSVA) was utilized to calculate the enrichment score of these oncogenic signatures in each sample of ICC [32]. For gene set enrichment analysis (GSEA), differentially expressed genes (DEGs) were identified using the "limma" package and ranked in descending order based on their fold change [33,34]. Both GSVA and GSEA were performed using the "clusterProfiler" package [35].

2.6. Evaluation of SS

Principal component analysis (PCA) [36] was used to construct a scoring system to estimate the levels of SRSGs in ICC patients, and termed as SS. The formula of SS was shown as followed:

$$SS = \sum(PC1 + PC2)$$

The correlations between SS and clinic, molecule and immune

characteristics were further evaluated in ICC samples.

2.7. Cell line and cell culture

Human ICC cell line RBE (TCHu179) was purchased from National Collection of Authenticated Cell Cultures (Shanghai, China), and human ICC cell line HUCCT1 was kept in Liver Cancer Institute, Zhongshan Hospital, Fudan University (Shanghai, China). RBE and HUCCT1 cells were maintained in RPMI-1640 medium (11875500, Gibco, New York, USA) with 10% fetal bovine serum (FBS; 10270–106, Gibco) and 1% penicillin-streptomycin (1719675, Gibco), being cultured at 37 ℃ in 5% CO2 in a humidified ThermoForma incubator (Thermo Fisher Scientific, Waltham, MA, USA).

2.8. 3D fibro gels culture of tumor-repopulating cells (TRC)

Huang et al. found that 3D fibrin gels could promote the selection and growth of TRC, a kind of CSLCs [37]. Hence, 3D fibrin gels were applied for the selection and cultivation of ICC-TRC. Specifically, 100 U/mL thrombin (SEA-135, Sea Run Holdings Inc.) diluted with T7 buffer (50 mM Tris-HCl, 150 mM NaCl, pH 7.4) was firstly added to the culture plate. RBE or HUCCT1 cells were trypsinized and resuspended in complete medium, and then mixed 1:1 with 2 mg/mL salmon fibrinogen (SEA-133, Sea Run Holdings Inc., Freeport, ME, USA) diluted with T7 buffer. Next, this mixture was mixed at a 1:50 ratio with thrombin in each well. After incubation for 30 min in a 37 ℃ humidified incubator, the 3D fibrin gels culture environment was constructed successfully. ICC-TRC were cultured in 3D fibrin gels for 72 h and then used for subsequent experiments. Dispase II (1 U/mL; 40104ES60, Yeasen, Shanghai, China) was used to digest 3D fibrin gels and collect ICC-TRC.

2.9. Quantitative reverse transcription polymerase chain reaction (qRT-PCR)

The mRNA level of target genes was determined using qRT-PCR. In detail, the mRNA of 2D cultured cells or ICC-TRC was extracted using RNA-Quick Purification Kit (RN001, ES Science, Shanghai, China), and then reversely transcribed into cDNA using Hifair® V one-step RT-gDNA digestion SuperMix Kit (11141ES60, Yeasen) according to manufacturer's instructions. Then, the conditions of qRT-PCR were set as follows: initial denaturation at 95 ℃ for 5 min, 40 cycles of 95 ℃ for 10 s and 60 ℃ for 30 s, which was performed using SYBR Green kit (11202ES08) on a QuantStudio5 fluorescence quantitative PCR system (Applied Biosystems, Foster City, CA, USA). The sequences of all primers were displayed in Table S6. Using GAPDH as the internal normalization, the $2^{\Delta\Delta CT}$ method was used to calculate the relative gene expression change.

2.10. Western blotting

Western blotting was used to perform the detection of proteins. The total proteins of 2D cultured cells or ICC-TRC was extracted using RIPA lysis buffer (P0013C, Beyotime Biotechnology, JiangSu, China) with 1 mM PMSF (20109ES05, Yeasen) and 1% Protease inhibitor (20124ES03, Yeasen). Proteins were separated by SDS-PAGE (10%), and further transferred to polyvinylidene difluoride (PVDF; ISEQ00010, Merck Millipore Ltd., Darmstadt, Germany). After blocked by QuickBlock™ Blocking Buffer (P0239, Beyotime Biotechnology) for 15 min, the membranes were incubated with the primary antibody (Table S7) at 4 ℃ overnight and then with the corresponding secondary antibody (Table S7) for 1 h at room temperature. Chemistar™ highsig ECL western blotting substrate (180–5001, Tanon, Shanghai, China) was used to visualize the protein bands on a Tanon 5200 Automatic Chemiluminescence Image Analysis System (Tanon).

2.11. Senescence-associated β-galactosidase (SA-β-Gal) staining

The activity of SA-β-Gal is an important biomarker for cell senescence [4]. To detect cell senescence, SA-β-Gal staining was performed by using senescence β-galactosidase staining kit (C0602) from Beyotime Biotechnology according to manufacturer's instructions.

2.12. Transwell assays

Invasion and migration ability of ICC-TRC was evaluated by transwell assays. To investigate the invasion ability, 50 μl matrigel (356234, BD Biosciences, New Jersey, USA) diluted at 1:8 with RPMI-1640 medium was added to the microporous membrane of Transwell Permeable Supports (3422, Corning Inc., New York, USA). After incubated at 37 ℃ for 4 h, 500 μl of RPMI-1640 medium containing 20% FBS was added to the lower chamber and 300 μl of RPMI-1640 medium with 3×10^4 pretreated cells to the upper chamber, and cultured at 37 ℃ for 48 h. The supports were took out and the cells above the microporous membrane were removed by cotton swab carefully. The cells passing through the membrane filter were stained with 0.1% crystal violet solution (V5265, Sigma, St. Louis, MO, USA). The invasive cells were recorded using microscope and counted by Image J soft (National Institutes of Health, Maryland, USA). For the investigation on migration ability, all of the processes were consistent to the above besides no matrigel used.

2.13. RNA interference

To silence the expression of *HELLS*, cells were transfected with siRNA by applying riboFECT™ CP (C10511–05, RIBOBIO, Guangdong, China). The targeted sequence of negative control (NC), siHELLS-1 and siHELLS-2 was, TTCTCCGAACGTGTCACGT, GCAGCAGATACAGTTATCA and GAACGTCAAAAATTGGTAA, respectively.

2.14. Human derived cell supernatant 9 cytokines detection assay

SASP is involved in the release of excessive bioactive cytokines, including chemokines, interleukins, and proteases. Accordingly, the level of 9 cytokines, including CCL5, HGF, IL1α, IL1β, IL-6, IL-8, TGFβ1, VEGF, CXCL1, was detected using ABplex Human 9-Plex Custom Panel (RK04338, Abclonal, Wuhan, China) in the supernatant of ICC cells or ICC-TRC. The detailed processes were as followed. Antibody molecules specific to different target molecules are covalently crosslinked to specific encoded microspheres, with each encoded microsphere corresponding to a specific detection assay. By liquid-phase reaction, fluorescently encoded microspheres specific to different target molecules are mixed and then added to the sample containing the target molecules. The resulting complex reacts with labeled fluorescein to generate a fluorescent signal. Under the driving force of flowing sheath fluid, microspheres pass through red and green lasers in a single-file formation. The red laser is applied for determining the fluorescent code of the microspheres, and the green laser for the fluorescence intensity of the reporting molecule on the microsphere. The detection was achieved using ABplex-100 (Abclonal).

2.15. Statistical analysis

All plots and statistical analyses were conducted using R version 4.3.0 or GraphPad Prism 8.0. Pearson correlation analysis was employed for correlation analysis. Clinical parameters were compared between groups using either the Chi-square test or Fisher's exact test. The t-test was used for normally distributed data, while the Mann-Whitney test for non-normally distributed data. OS was defined as the time from diagnosis to the last follow-up or death, while relapse-free survival (RFS) as the time from diagnosis to the last follow-up or recurrence. Most cellular experiments were performed independently three times, and the t-test was used as the statistical method. A *p*-value less than 0.05 was

considered statistically significant, unless otherwise indicated.

3. Results

3.1. SRSGs-related classification was associated with the prognosis of ICC

The data of RNA-seq and microarray were merged to enlarge the sample size. After removing the batch effects *via* "sva" package [38], the stemness indices were calculated in ICC using ssGSEA and OCLR algorithms (Table S4). Setting the threshold values as followed: |Pearson correlation coefficient (PCC)| > 0.3 and $p < 0.05$, SRGs significantly associated with two stemness indices were considered as SRSGs (n = 14) in ICC (Table S8, Fig. 1A and B). The top 10 enrichment of biological process (BP), molecular function (MF), and cellular component (CC) was mainly involved in DNA damage and repair, cell cycle as well as chromatin conformation (Fig. S2). KEGG analysis indicated that these genes mainly enriched in cellular senescence, cell cycle, base excision repair, platinum drug resistance and DNA replication (Fig. S2). Then, ICC samples were divided into C1 and C2 type using a unsupervised clustering based on the SRSGs (Fig. S3). The SRSGs-related classification was significant association with Ahn's and Anderson's classification in ICC (Table S9 and Fig. 1C) [18,23]. In particular, C2 type of ICC had a higher proportion of SG III-IV ($p < 0.0001$) and class B ($p < 0.01$) type of ICC (Fig. 1C). Survival analysis indicated that C2 suffered a shorter mOS than C1 (24.3 months *vs.* not reached, $p = 0.011$) in the combined cohort (CHOL, GSE89749 and GSE107943 cohorts; Fig. 1D). Similar results were observed in CHOL cohort (24.3 months *vs.* not reached, $p = 0.024$), while C2 only had a trend of poor prognosis in GSE89749 (18.6 months *vs.* not reached, $p = 0.33$) and GSE107943 (26.4 *vs.* 38.3 months, $p = 0.19$) cohort (Fig. S4). In addition, C2 had a shorter median RFS (mRFS) than C1 (6.9 *vs.* 21.9 months, $p = 0.025$) in GSE107943 cohort (Fig. S4). Clinical analysis showed that the classification was significant association with HBV infection in GSE89749 cohort, with a higher infection rate in C1 type (27.6% *vs.* 3.4%, $p = 0.012$; Fig. 1E). Taken together, the SRSGs-related classification may be an independent prognosis signature for ICC.

3.2. The immune, molecule and metabolism characteristics in the two subclasses of ICC

Cell senescence, especially SASP plays a crucial role in cancer immunity [6]. The results of ESTIMATE algorithm showed that C1 type of

Fig. 1. SRSGs-related classification of ICC. A & B. OCLR and ssGSEA were employed to measure the stemness indices of ICC. Pearson correlation analysis was used to evaluate the correlation between stemness indices and SRGs in ICC. Total 14 SRGs were identified as SRSGs with significant correlation with the two stemness indices. C. Correlation of SRSGs-related classification (C1 and C2) with previous ICC subclasses in the ICC samples. D. OS of two clusters (C1 and C2) in ICC samples. E. Correlation of SRSGs-related classification (C1 and C2) with clinic features in the different ICC cohorts. OCLR, one class linear regression; ssGSEA, single sample gene set enrichment analysis; ICC, intrahepatic cholangiocarcinoma; PCC, Pearson correlation coefficient; SRSGs, senescence-related stemness genes.

ICC had a higher immune score ($p < 0.05$), stromal score ($p < 0.0001$), estimate score ($p < 0.001$), but a lower tumor purity ($p < 0.001$) than C2 (Fig. 2A). The results of xCell showed that C1 type of ICC had a high immune score ($p < 0.05$), stromal score ($p < 0.0001$), as well as microenvironment score ($p < 0.0001$). These data suggested that C1 type of ICC may stay in a more active TME. Further data from MCPcounter indicated that both immune cells (NK cells, T cells, B lineage and Myeloid DC) and stromal cells (endothelial cells and fibroblasts) were enriched in C1 type of ICC (Fig. 2B). Other algorithm also confirmed that most of TME cells were enriched in C1 type of ICC, yet rare in C2 type of ICC, including Macrophage M0, T cells CD4 + memory activated, T cells CD4 + memory rest and uncharacterized cells (Fig. 2C). These data suggested a high immune and stromal cell infiltration in C1 type of ICC. Moreover, the data of TIDE algorithm showed that although C1 type of ICC had a higher dysfunction score than C2 type of ICC, no significant differences were observed when compared exclusion and TIDE score (Fig. 2A). Cancer immune cycle was considered as the major steps for immune response. The results showed that most of immune steps were enriched in C1 type of ICC, including step 2, 3,6 and 7 (Fig. 2C). We also investigated the recruitment of immune cells (step 4) in ICC, and found that more recruitment occurred in C1 type of ICC. In a word, C1 type of ICC had a high immune infiltration and stayed at an immunostimulation TME.

Next, the molecular characteristics were evaluated in the two subclasses of ICC. GSEA of the hallmark gene set and KEGG demonstrated that the up-regulated genes in C1 type of ICC were enriched in multiple carcinogenesis associated pathways, including EMT, angiogenesis, KRAS signaling, JAK/STAT signaling pathway, TGF beta signaling pathway *etc*. (Fig. 3A). Several immune-related pathway, such as chemokine signaling pathway, B cell receptor signaling pathway, cytokine-cytokine receptor interaction, complement and coagulation cascades, was also enriched in C1 type of ICC (Fig. 3A), accounting for the high immune infiltration. In C2 type of ICC, we observed more cell cycle related pathway (such as E2F targets, G2M checkpoint, P53 signaling pathway, MYC targets, mitotic spindle), as well as DNA replication and damage repair related pathways (Fig. 3A). The results from GSVA also conducted a similar observation (Fig. 3B). These data suggested that the two subclasses had significantly distinct molecular characteristics.

Moreover, the metabolism characteristics were explored in the two subclasses of ICC. In general, we found that more metabolism processes were significantly enriched in C2 type of ICC, including nucleotide metabolism (folate one carbon metabolism, purine biosynthesis, purine metabolism, amino sugar and nucleotide sugar metabolism, folate biosynthesis, pyrimidine metabolism), lipid metabolism (fatty acid elongation, fatty acid biosynthesis, cholesterol biosynthesis, glycerophospholipid metabolism, steroid biosynthesis) as well as glucose metabolism (starch and suctose metabolism, glycogen biosynthesis, pentose phosphate pathway, fructose and mannose metabolism, glycolysis gluconeogenesis, galactose metabolism; Fig. 3C). Only 15 metabolism processes were significantly enriched in C1 type of ICC, including amino acid metabolism (tryptophan metabolism, histidine metabolism, beta alanine metabolism), and bile acid metabolism (Fig. 3C). Comparatively, C2 type of ICC performed as a high metabolism tumor.

3.3. The clinical significance of SS

Above results confirmed the association of cell senescence with ICC's immunity, metabolisms and prognosis. Based on these SRSGs, a scoring model was established to measure the level of cell senescence in ICC patients. The PCA analysis of a combined cohort (CHOL + GSE107943 + GSE89749) showed that the variance contribution rate of the first two principal components is of significant importance (Fig. S5A). Hence, the sum of PC1 and PC2 was determined to be the SS for each samples (Table S10). Comparing the SS between the two subsclasses, we found that C2 had a significantly higher SS than C1 (Fig. 4A and B). The SS had a significantly positive correlation with most of SRSGs (*BRCA1*, *CCNA2*, *CHEK2*, *FEN1*, *FOXM1*, *HELLS*, *HMGB2*, *HSPD1*, *LMNB1*, *PCNA*, *TOP2A*, and *TXN*), but negative with *EPOR* (Table S11). Next, the "Survminer" package of R was used to determine the optimal cutoff of SS in the combined cohort (Fig. S5). Accordingly, samples were divided into high (HSS) or low SS (LSS) groups. LSS group had a longer mOS than HSS group in the combined cohort (23.4 *vs* 46.0 months, $p = 0.025$; Fig. 4C). HSS group also performed a significantly poorer prognosis in the RNA-seq cohort (CHOL + GSE107943; 24.7 *vs* 46.7 months, $p = 0.039$), and a tendency toward worse prognosis in GSE89749 cohort (18.1 *vs* 46.0 months, $p = 0.17$; Fig. S6). LSS group possessed a longer mRFS than the HSS group in GSE107943 cohort (5.9 *vs* 21.9 months, $p = 0.00018$; Fig. 4D). In addition, we compared the efficacy of SS and previous risk score for predicting prognosis of ICC [39]. The results showed that the prediction efficacy of SS was comparable to Wang's risk score (Fig. S7). These data suggested that this SS may be a promising prognosis index for ICC.

The role of SS was further explored in oncogenic signatures, metabolisms, and immunity. At first, SS was positive association with both ssGSEA stemness index and mRNAsi (Fig. 4E), indicating that cell senescence may boost cancer stemness in ICC. Next, according to the thresholds ($|PCC| > 0.3$, $p < 0.05$), SS was positive association with G2M checkpoint, E2F targets, Mtorc1 signaling, MYC targets, P53 signaling pathway, PI3K/AKT/MTOR signaling, but negative relation to Hedgehog signaling (Fig. 4F). SS was also positively related to DNA repair and replication related process, as well as cell cycle (Fig. 4G). It is notable that SS was negative association with two crucial hallmarks of cancer in ICC, that is EMT and angiogenesis (Fig. 4G). In addition, our results showed that SS was positive association with majority of metabolisms ($p < 0.05$; Fig. 4H). What's more, we found that the higher SS, the more infiltration of cells, including CD4 T cells, CD8 T cells, Th2 cells, DC and macrophage, in ICC (Fig. 4I). The SS was negative association with NK cells and stromal cells (endothelial cells and fibroblasts). We also analyzed some immune-related pathways in ICC and majority of these pathways were enriched in HSS group (Fig. 4J). The results of TIDE indicated that SS was significantly negative correlation with dysfunction, exclusion as well as TIDE score (Fig. 3K), prompting that tumor in HSS group may had a more active immune environment. Of note, our results showed that LSS group displayed a significantly lower response rate to immunotherapy than HSS group (Fig. 4L). Finally, we evaluated the relationship between SS and mutation, but no significant differences were observed (Fig. S8). In summary, SS was closely related to the oncogenic signatures, metabolisms, and immunity of ICC.

3.4. ICC-TRC displayed a more activity SASP

In order to confirm the function of cell senescence in ICC, ICC-TRC were selected using 3D fibrin gels. The data indicated more active SA-β-Gal in HUCCT1-TRC or RBE-TRC than in HUCCT1 or RBE cells, implying more cell senescence occurred in ICC-TRC (Fig. 5A). As abovementioned, SASP displayed a close involvement in CSLCs due to its release of excessive bioactive factors, such as chemokines, interleukins, and proteases [3,7]. To this end, the level of bioactive cytokines was detected using cytokines detection assay and western blotting in ICC. We found that chemokines (CCL5, CXCL1), interleukins (IL1α, IL1β, IL6), transforming growth factors (TGF-β1), matrix metalloproteinases (MMP3, MMP10), growth factors (VEGF, HGF, CTGF) and cell adhesion molecules (ICAM1) were obviously increased in ICC-TRC when compared with 2D cultured ICC cells (Figs. 5B and 5C), indicating an active SASP in ICC-TRC.

3.5. HELLS was a key senescence-related stemness gene in ICC

The clinical significance of the 14 genes was analyzed in ICC to further identify the critical SRSGs. Setting median value as the cutoff value, we found that only *CHEK2*, *HMGB2*, *TOP2A*, *HELLS*, and *EPOR*

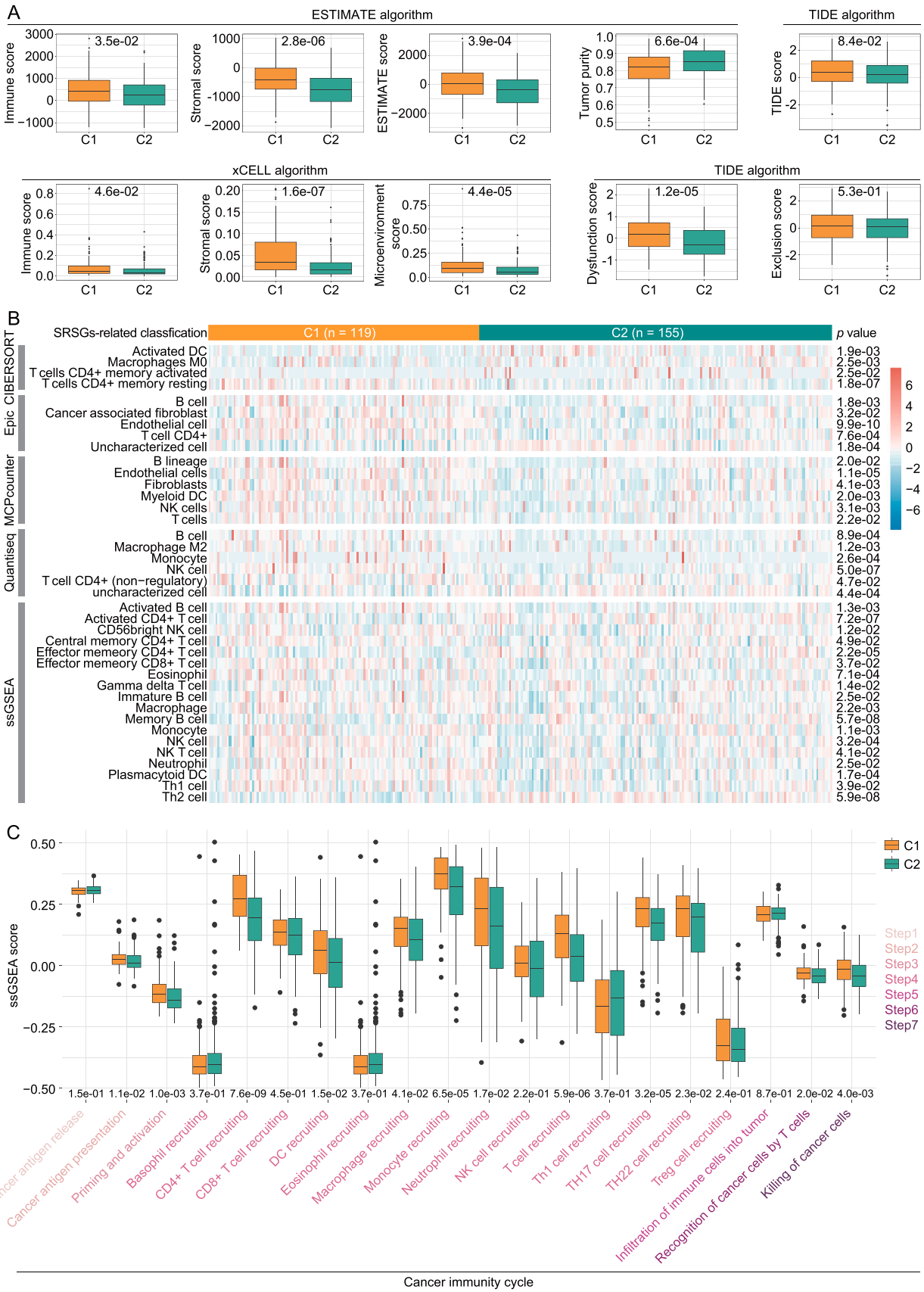

Fig. 2. Different ICC subclasses showed a distinct tumor microenvieronment. A. The overall immune status between different ICC subclasses was assessed by using Estimate and TIDE algorithm. B. Immune infiltration analysis of the different ICC subclasses. C. The immunity cycle analysis of the different ICC subclasses. ICC, intrahepatic cholangiocarcinoma; TIDE, tumor immune dysfunction and exclusion.

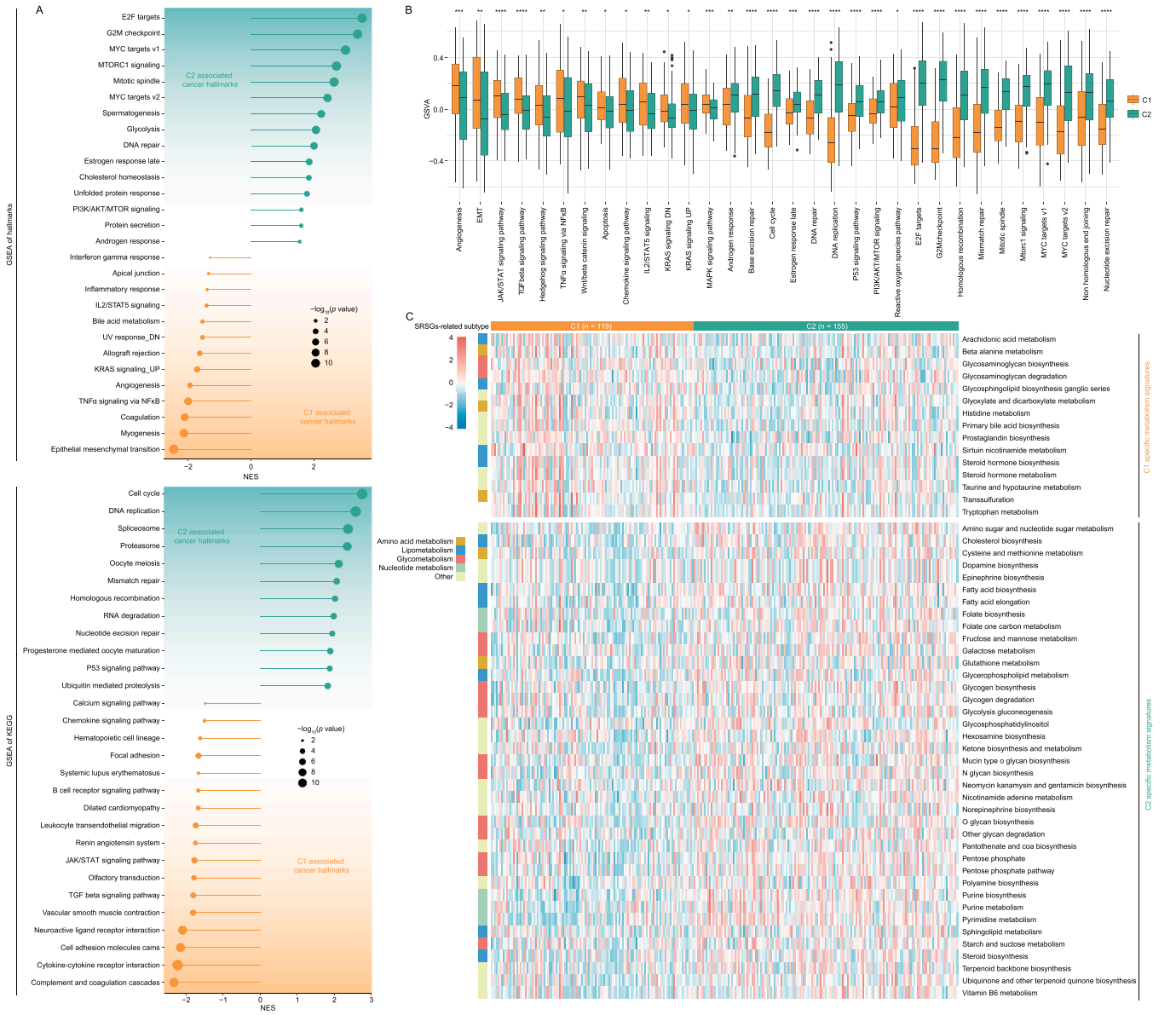

Fig. 3. The molecular and metabolism characteristics in different ICC subclasses. A & B. GSEA (A) and GSVA (B) analysis of the different ICC subclasses. C. Heatmap of the specific metabolism-associated signatures in ICC. ICC, intrahepatic cholangiocarcinoma; GSEA, gene set enrichment analysis; GSVA, gene set variation analysis.

were significantly association with ICC's RFS (Fig. 6A and Fig. S9). Patients with high expression of *CHEK2* (6.5 *vs.* 21.9 months, $p = 0.028$), *HMGB2* (6.5 *vs.* 21.9 months, $p = 0.015$), *TOP2A* (6.9 *vs.* 21.9 months, $p = 0.012$) or *HELLS* (6.9 *vs.* 21.9 months, $p = 0.04$) suffered a shorter mRFS than those with low expression, while contrary in comparing *EPOR* (21.9 *vs.* 5.9 months, $p = 0.0012$). After the cutoff value being optimized by the "Survminer" package of R (Fig. S10), the survival analysis indicated that only *HMGB2*, *TOP2A* and *HELLS* were significantly association with ICC's OS (Fig. 6A). Among which, high expression of *TOP2A* (24.3 months *vs.* Not reached, $p = 0.012$) or *HELLS* (24.9 *vs.* 46.0 months, $p = 0.0059$) showed a shorter mOS than those with low expression, while reverse in comparing *HMGB2* (37.3 *vs.* 18.9 months, $p = 0.028$). Overall, *CHEK2*, *HMGB2*, *TOP2A*, and *HELLS* were positive related to stemness, up-regulated in ICC, and positive associated with RFS, but *EPOR* on the contrary (Fig. 6B). Data from qRT-PCR showed that *HELLS* significantly up-regulated in both HUCCT1-TRC and RBE-TRC compared to HUCCT1 or RBE, but other 4 genes didn't (Fig. 6C). The protein level of HELLS was also up-regulated in ICC tissues (Fig. 6D; the data of immunohistochemistry were from the Human Protein Atlas database, https://www.proteinatlas.org/) [40]. The results of western blotting demonstrated that the protein of HELLS in ICC-TRC was higher than that in 2D cultured cells (Fig. 6E). Accordingly, *HELLS* was considered as a critical SRSGs involved in stemness and prognosis in ICC.

3.6. *HELLS promotes the malignant behaviors of ICC-TRC via activating SASP*

Finally, the biologic function of HELLS was evaluated in ICC-TRC. The data of western blotting indicated a good silence effect of siRNA against HELLS in HUCCT1-TRC and RBE-TRC (Fig. S11). Silencing HELLS significantly decreased the migration and invasion ability, and inhibited the growth of colony in both HUCCT1-TRC and RBE-TRC (Fig. 7A and B), indicating that HELLS played a crucial role in promoting malignant behaviors of ICC-TRC. However, silencing HELLS didn't cause a significant alteration on the activity of SA-β-Gal in ICC-TRC (Fig. 7C). Further studies found that silencing HELLS significantly

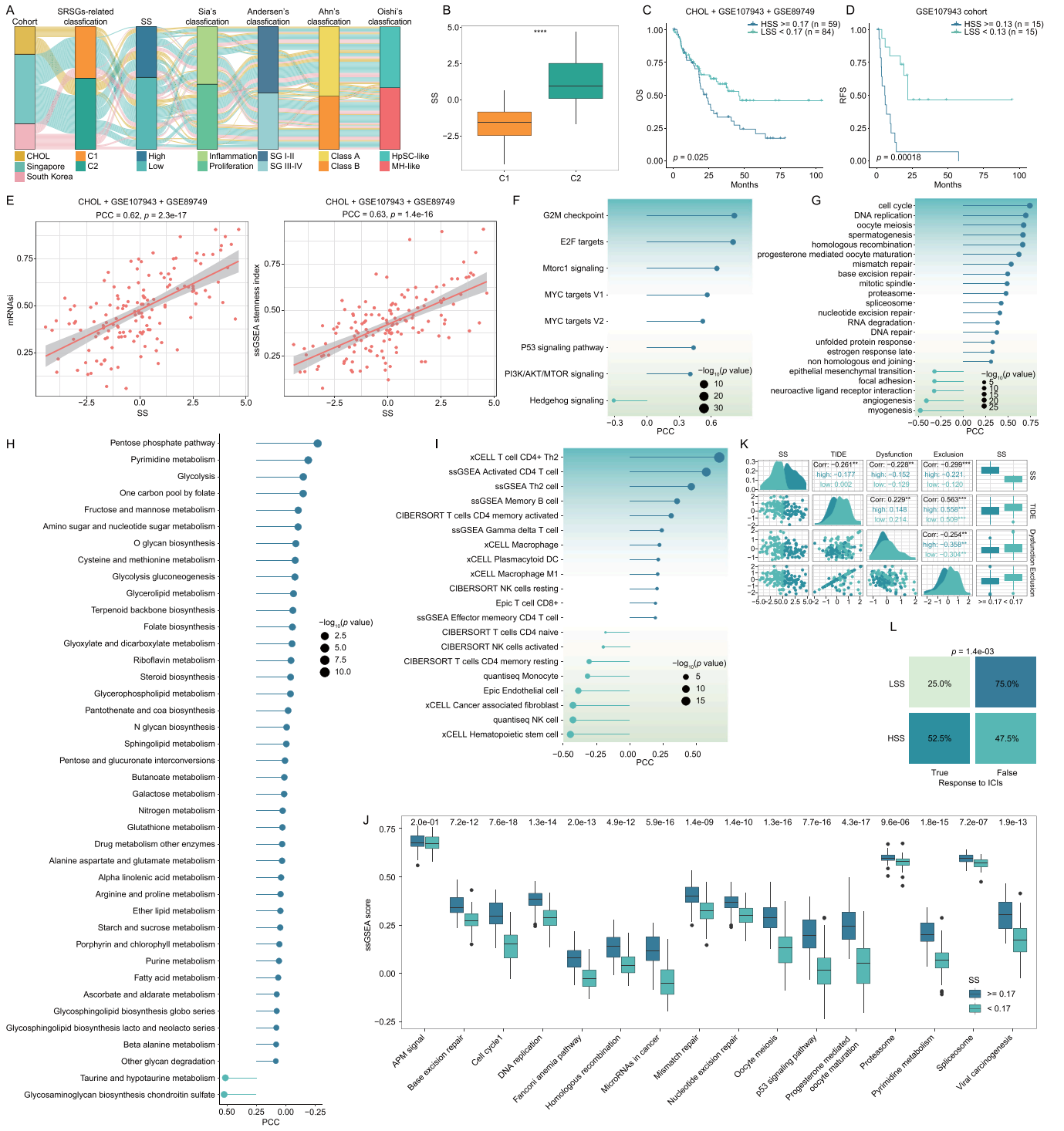

Fig. 4. Association between SS and stemness indices, clinic and molecular features in ICC. A & B. SS in different ICC sunclasses. C & D. OS (C) and RFS (D) of different SS groups (HSS, LSS). E-I. Correlation analysis between SS and stemness indices (E), oncogenic pathways (F), oncogenic signatures (G), metabolism processes (H), and immune infiltration (I). J. The ssGSEA score of immune-related pathways in different SS groups (HSS and LSS). K. TIDE analysis of different SS groups (HSS and LSS). L. The response rate to immunotherapy of the different SS groups (HSS and LSS) was predicted by using TIDE analysis. SS, senescence score; ICC, intrahepatic cholangiocarcinoma; OS, overall survival; RFS, relapse-free survival; HSS, high senescence score; LSS, low senescence score; ssGSEA, single sample gene set enrichment analysis; TIDE, tumor immune dysfunction and exclusion.

decreased the expression of multiple bioactive factors, such as ICAM1, MMP3, MMP10, AREG and CTGF (Fig. 7D), which were up-regulated in ICC-TRC. It also significantly decreased the secretion of IL1α, IL1β, IL6, IL8, CXCL1, TGF-β1 and VEGF in HUCCT1-TRC, while it significantly inhibited all detected cytokines in RBE-TRC (Fig. 7E). These data suggested that HELLS may drive the malignant behaviors of ICC-TRC *via* promoting SASP, and decreasing it could inhibit SASP.

4. Discussion

Bioinformatics methods were utilized to identify 14 genes that are related to both cell senescence and stemness, collectively referred to as

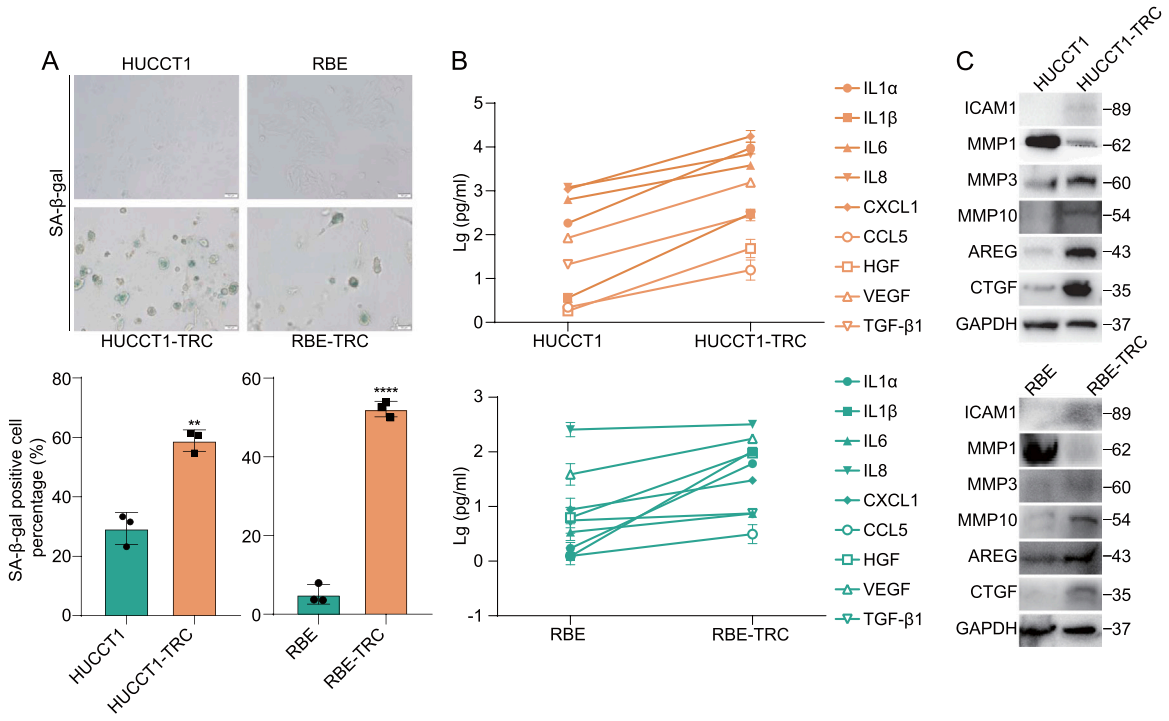

Fig. 5. Increased SASP in ICC-TRC. A. Cell senescence was detected by SA-β-gal staining in HUCCT1, HUCCT1-TRC, RBE, and RBE-TRC (mean ± SD, n = 3, t-test). B. The level of bioactive factors in the cell supernatant (mean ± SD, n = 3, t-test). The concentration of bioactive factors was normalized with 1×10^6 cells. C. The level of bioactive factors were detected by western blotting in HUCCT1, HUCCT1-TRC, RBE, and RBE-TRC. SASP, senescence-associated secretory phenotype; ICC, intrahepatic cholangiocarcinoma; TRC, tumor-repopulating cells; SA-β-Gal, senescence-associated β-galactosidase; SD, standard deviation.

SRSGs. Based on the 14 SRSGs, ICC samples were clustered into two distinct types (C1 and C2) using a consensus clustering. The C1 type of ICC was characterized by enriched immune cell infiltration, amino acid metabolism, bile acid metabolism, and a favorable prognosis, while the C2 type of ICC exhibited enriched nucleotide metabolism, lipid metabolism, glucose metabolism, and a poor prognosis. Moreover, a prognosis score was calculated using PCA of the 14 SRSGs, and we observed a positive correlation between SS and stemness in ICC. With SS increased, we noticed a corresponding increase in immune infiltration, metabolism, and oncogenic signatures in ICC. Patients with a high SS have a poor prognosis, but may respond well to immunotherapy. Finally, we identified *HELLS* as a key gene in ICC-TRC that may promote malignant behaviors by enhancing the SASP.

Cell senescence has been confirmed as a crucial hallmark for cancers [4]. One illuminating case study was that the depletion of senescent cells in aging mice reduced the incidences of spontaneous tumorigenesis and cancer-associated death [41]. Its driving action to cancers can be summarized into the following three parts: 1) SASP of senescent cancer cells yield a massive bioactive factors, and thereby affect the adjacent viable cancer cells, as well as other cells of TME *via* a paracrine manner, contributing to cell proliferation, apoptosis resistance, angiogenesis, invasion and metastasis, and tumor immunosuppression; 2) Senescent cancer cells can exit from their SASP and nonproliferative status, and restore associated capabilities necessary for viable oncogenic cells; 3) Senescence occurred in other cells of TME is also a driving force for tumor evolution [4]. Previous studies established different SRGs-related risk score models in osteosarcoma, bladder cancer, and colorectal cancer [42–44]. They provided comprehensive insights into the correlation between cell senescence and tumor immunity, clinical prognosis or some other cancer features. Different from these studies, we focused on SRGs that were significantly associated with stemness of ICC, which were termed as SRSGs (*BRCA1*, *CCNA2*, *CHEK2*, *FEN1*, *FOXM1*, *HELLS*, *HMGB2*, *HSPD1*, *LMNB1*, *PCNA*, *TOP2A*, and *TXN*), and accordingly, a novel classification was established for ICC. Compared with previous classification, the new classification showed a independent predict value for prognosis. Significant differences were observed on oncogenic signatures and metabolisms between the different classification of ICC (C1 and C2). In addition, based on the 14 SRSGs, a prognosis risk score — SS was established by PCA. Similarly, we found that SS was significantly correlation with stemness, metabolisms, oncogenic signatures, as well as prognosis. The results supported the viewpoint that cell senescence has a close involvement in cancers. These new classification and new risk score may contribute to the prognostic evaluation and treatment guidance of ICC.

Of note, cell senescence played a crucial role in cancer immunity [45, 46]. The senescence of immune cells could be induced by many factors in cancer, such as cAMP, glucose competition, and oncogenic stress in the TME [45]. The senescent cells are not limited to T cells, also include B cells, macrophages, NK cells, and DC, which is linked to the occurrence and progression of tumors [45]. C2 type of ICC that had a relative high level of SRSGs showed a significantly silent immune TME compared to C2 type, indicating that cell senescence also affected the cancer immunity of ICC. However, HSS group had a higher level of immune infiltration than LSS group, including multiple immune cells infiltration, which seems be inconsistent with previous studies. The possible causes should be that we established this risk score model only based on the expression of SRSGs, yet ignored the function of SASP in TME. SASP could affect cancer immunity *via* regulating immune surveillance, immune evasion as well as matrix remodeling [46]. In detail, it could regulate the infiltration of cells in TME and modulated their functions [46]. In addition, SASP could enhance the benefit from immunotherapy [46]. Our data indicated that HSS group had a higher response rate to immunotherapy than LSS group. Therefore, we inferred that HSS group may had a more active SASP (data not shown).

Additionally, we found that more cell senescence occurred in ICC-TRC than in 2D cultured ICC cells. Previous study indicated that cell senescence could promote stemness in lymphoma, multiple myeloma and hepatocellular carcinoma [7–9]. Further results showed that

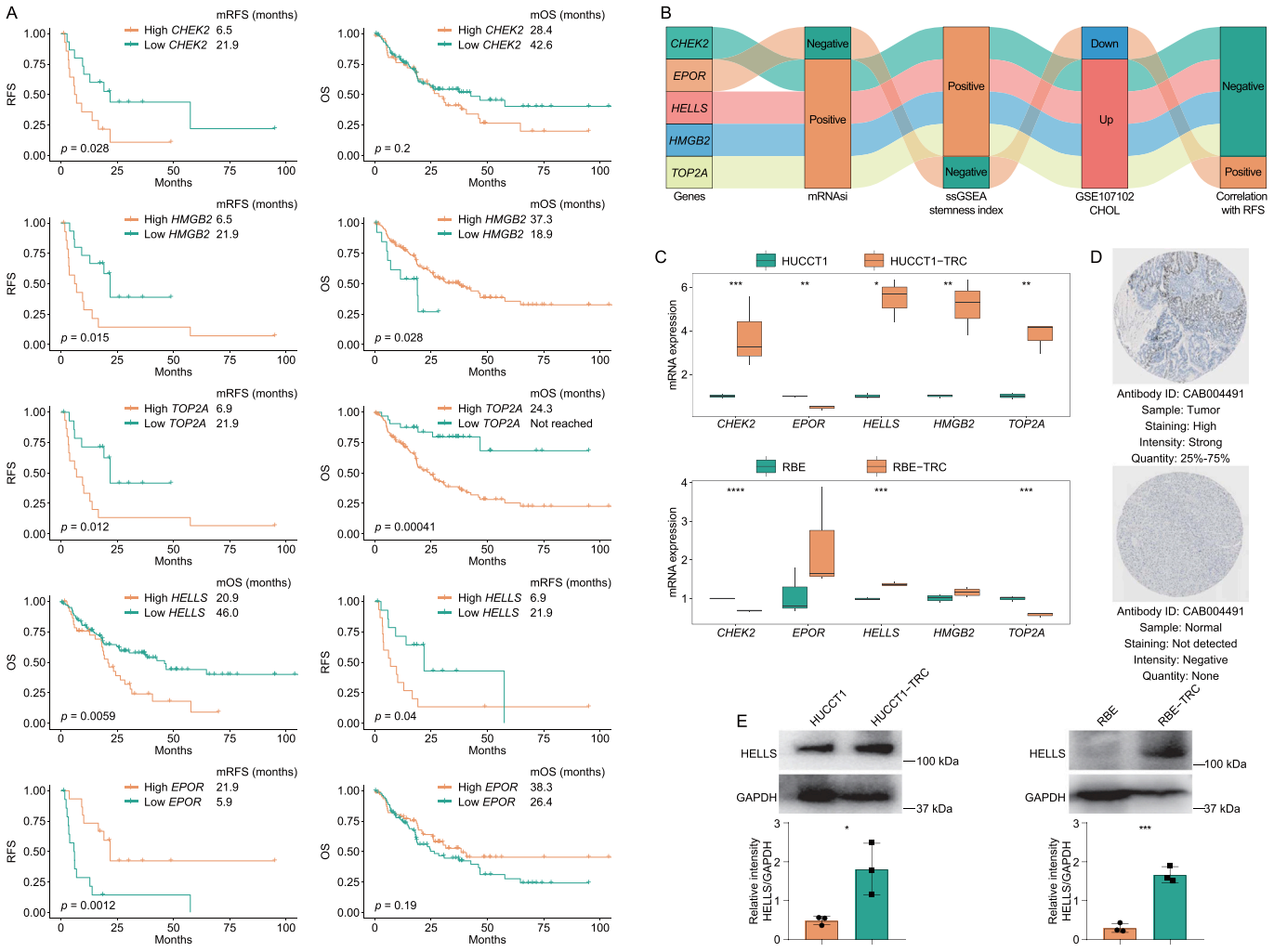

Fig. 6. HELLS was up-regulated in ICC-TRC. A. OS and RFS of different ICC groups clustered by the expression of *CHEK2*, *HMGB2*, *TOP2A*, *HELLS* or *EPOR*. B. The sankey plot showed that correlation between the 5 genes (*CHEK2*, *HMGB2*, *TOP2A*, *HELLS*, *EPOR*) and stemness indices and RFS, as well as their expression in ICC. C. The mRNA of the 5 genes (*CHEK2*, *HMGB2*, *TOP2A*, *HELLS*, *EPOR*) was detected by qRT-PCR in HUCCT1, HUCCT1-TRC, RBE, and RBE-TRC (mean ± SD, n = 3, t-test). D. The protein level of HELLS in ICC and normal bile duct tissues. E. The expression of HELLS was detected by western blotting in HUCCT1, HUCCT1-TRC, RBE, and RBE-TRC. The data was analyzed by Image J (mean ± SD, n = 3, t-test). ICC, intrahepatic cholangiocarcinoma; TRC, tumor-repopulating cells; SD, standard deviation; OS, overall survival; RFS, relapse-free survival.

ICC-TRC yields more bioactive factors, such as chemokines, interleukins, and MMPs, *etc.*, indicating that it had a more active SASP. Hence, we infer that SASP may promote the stemness of ICC. Moreover, we found that a key SRSGs, named *HELLS*, was up-regulated, positive correlation with stemness, negatively related to prognosis in ICC, and up-regulated in ICC-TRC. HELLS is affiliated to a subfamily of the conserved SNF2 ATP-dependent chromatin-remodeling complexes, which could change the nucleosome structure and chromatin packaging during the processes of DNA replication, transcription, and repair *via* using energy from ATP hydrolysis [47]. It has been implicated in numerous cancers, including leukemia, colorectal cancer, retinoblastoma, glioblastoma, pancreatic cancer, nasopharyngeal carcinoma, lung cancer, breast cancer, and hepatocellulfar carcinoma [47]. HELLS acts as a driving role in these cancers *via* various mechanisms, such as sustaining proliferative signaling, promoting invasion and migration, driving epigenetic/genomic instability, evading cell death, and influencing metabolisms [47]. Our data demonstrated that silencing HELLS significantly inhibits the growth, invasion and migration of ICC-TRC. It's down-regulation also attenuates the secretion of most bioactive factors of ICC-TRC. Accordingly, HELLS may promote the malignant behaviors in ICC-TRC *via* boosting SASP. Of note, silencing HELLS hardly affects the cell senescence proportion in ICC-TRC. A mice experiment showed that disruption of LSH (murine orthologue of HELLS) caused a premature aging phenotype [48]. The difference may be explained by the disparate test subjects: we focused on the cell senescence in CSLCs, while they studied the aging mechanisms of mice. Hence, we inferred that the increased cell senescence in ICC-TRC may not caused by the up-regulated HELLS. Down-regulating HELLS may only decreased the secretion of bioactive factors, but not affect the senescence in ICC-TRC. On the foundation of silencing HELLS, inducing senescence may be a promising strategy for killing CSLCs in ICC. Taken together, HELLS may be a crucial factor for maintaining SASP, but not for inducing cell senescence in ICC-TRC.

There remain some problems to be solved. First, it is unclear why cell senescence was increased in ICC-TRC. Second, the mechanisms underlying HELLS mediated SASP have not been clarified yet. Third, SASP was considered as a clear mechanism of resistance in cancers [5]. It remains unclear whether silencing HELLS could overcome the resistance to oncotherapy.

5. Conclusions

In this study, we discovered a set of SRSGs in ICC. Based on these genes, we developed a new classification system and a risk score for ICC.

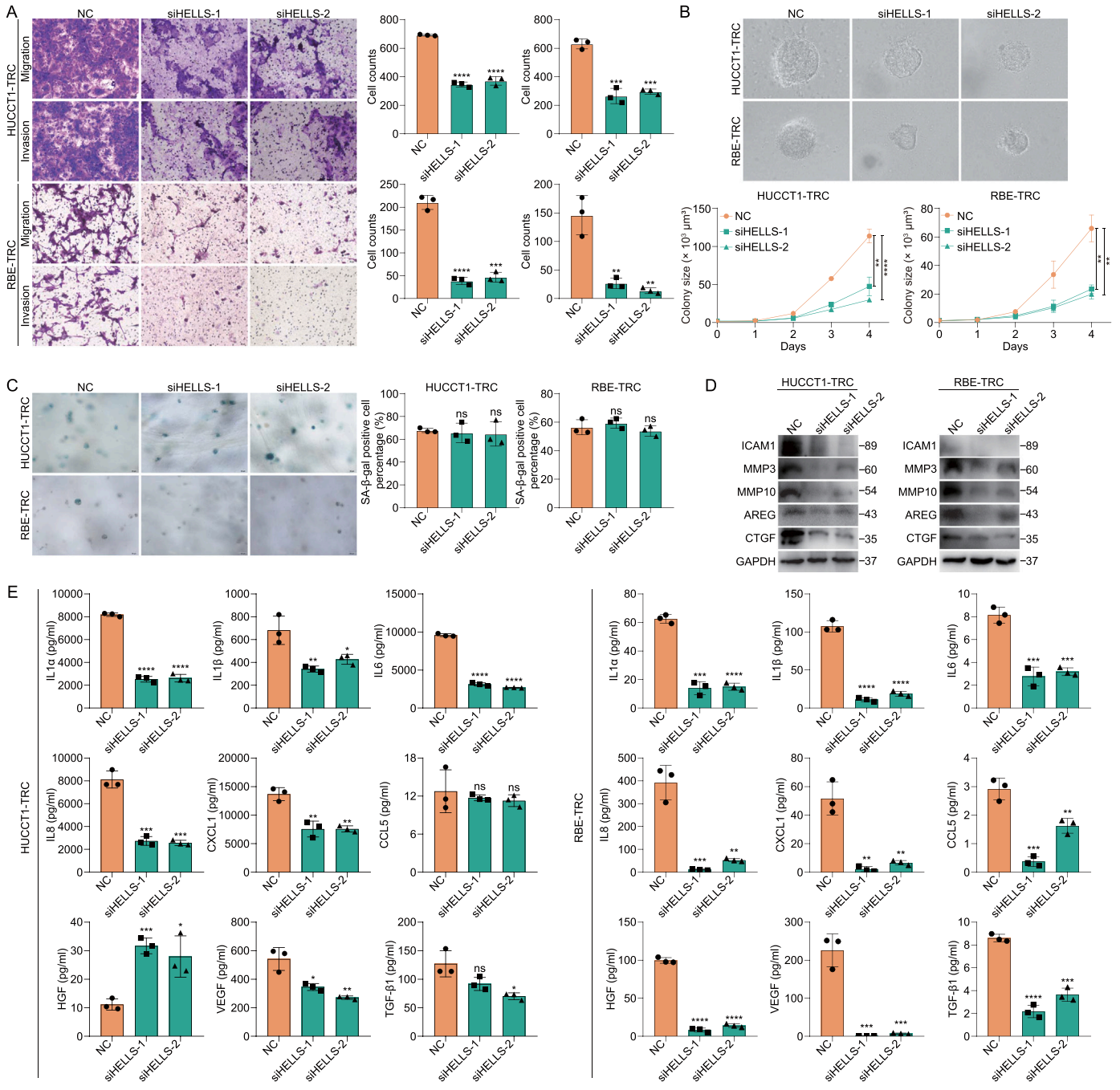

Fig. 7. Silencing HELLS decreased the malignant behaviours and SASP of ICC-TRC. A. Effect of silencing HELLS on the migration and invasion ability of ICC-TRC (mean ± SD, n = 3, t-test). B. Effect of silencing HELLS on the colony growth of ICC-TRC (mean ± SD, n = 3, t-test). C. SA-β-gal staining showed the effect of silencing HELLS on cell senescence of ICC-TRC (mean ± SD, n = 3, t-test). D. Effect of silencing HELLS on the level of bioactive factors in ICC-TRC. E. Effect of silencing HELLS on the level of bioactive factors in the cell supernatant (mean ± SD, n = 3, t-test). The concentration of bioactive factors was normalized with 1×10^6 cells. SASP, senescence-associated secretory phenotype; ICC, intrahepatic cholangiocarcinoma; TRC, tumor-repopulating cells; SA-β-Gal, senescence-associated β-galactosidase; SD, standard deviation.

We observed that these SRSGs are strongly correlated with prognosis, immunity, and metabolism in ICC. Further investigation of these genes may provide a deeper understanding of the molecular mechanisms of ICC. Additionally, we discovered that *HELLS* plays a crucial role in promoting SASP and malignant behaviors in ICC-TRC. These findings provide a novel strategy for targeting senescence to inhibit CSLCs in ICC.

Funding information

This study was funded by the Natural Science Foundation of Shanghai (20ZR1410400), National Natural Science Foundation of China (81972233, 81772590 and 81572395), and the Open Funding of Key Laboratory of Diagnosis and Treatment of Severe Hepato-pancreatic Diseases of Zhejiang Province (2018E10008).

Authors statement

All authors declare that none of any part of this manuscript has been published or is under consideration for publication elsewhere, including the internet. All authors declare no conflict of interest in this work.

CRediT authorship contribution statement

XD, XZ and ZQ contributed to the bioinformatics analysis and cellular experiments. YX was responsible for the data download and figures layout. XD wrote the manuscript. ZY, XC and JX provided the project idea, technical guidance, and guided manuscript revision.

Declaration of Competing Interest

The authors declare no conflict of interest.

Data Availability

Human RNA-seq data and microarray data were downloaded from TCGA (https://portal.gdc.cancer.gov/) and GEO (https://www.ncbi.nlm.nih.gov/geo/) database. SRGs were downloaded from HAGR (https://www.genomics.senescence.info/) database. Cancer immunity cycle related gene sets and enrichment gene sets (c2.cp.kegg.v7.4.symbols and h.all.v7.5.1.symbols) were obtained from the TIP website and MSigDB, respectively. The immunohistochemistry image of ICC tissues and normal tissues were from HPA (https://www.proteinatlas.org/) database.

Appendix A. Supporting information

Supplementary data associated with this article can be found in the online version at doi:10.1016/j.csbj.2023.09.020.

References

[1] Moris D, Palta M, Kim C, Allen PJ, Morse MA, Lidsky ME. Advances in the treatment of intrahepatic cholangiocarcinoma: an overview of the current and future therapeutic landscape for clinicians. CA Cancer J Clin 2023;73(2):198–222.
[2] Valle J, Wasan H, Palmer DH, Cunningham D, Anthoney A, Maraveyas A, et al. Cisplatin plus gemcitabine versus gemcitabine for biliary tract cancer. New Engl J Med 2010;362:1273–81.
[3] Mcgrath NA, Fu J, Gu SZ, Xie C. Targeting cancer stem cells in cholangiocarcinoma (Review). Int J Oncol 2020;57(2):397–408.
[4] López-Otín C, Pietrocola F, Roiz-Valle D, Galluzzi L, Kroemer G. Meta-hallmarks of aging and cancer. Cell Metab 2023;35(1):12–35.
[5] Chambers CR, Ritchie S, Pereira BA, Timpson P. Overcoming the senescence-associated secretory phenotype (SASP): a complex mechanism of resistance in the treatment of cancer. Mol Oncol 2021;15:3242–55.
[6] Takasugi M, Yoshida Y, Ohtani N. Cellular senescence and the tumour microenvironment. Mol Oncol 2022;16:3333–51.
[7] Milanovic M, Fan DNY, Belenki D, Däbritz JHM, Zhao Z, Yu Y, et al. Senescence-associated reprogramming promotes cancer stemness. Nature 2018;553:96–100.
[8] Karabicici M, Alptekin S, Fırtına Karagonlar Z, Erdal E. Doxorubicin-induced senescence promotes stemness and tumorigenicity in EpCAM-/CD133- nonstem cell population in hepatocellular carcinoma cell line, HuH-7. Mol Oncol 2021;15:2185–202.
[9] Cahu J, Bustany S, Sola B. Senescence-associated secretory phenotype favors the emergence of cancer stem-like cells. Cell Death Dis 2012;3:e446.
[10] Tacutu R, Thornton D, Johnson E, Budovsky A, Barardo D, Craig T, et al. Human Ageing Genomic Resources: new and updated databases. Nucleic Acids Res 2018;46:D1083–90.
[11] Malta TM, Sokolov A, Gentles AJ, Burzykowski T, Poisson L, Weinstein JN, et al. Machine learning identifies stemness features associated with oncogenic dedifferentiation. Cell 2018;173:338–54. e15.
[12] Barbie DA, Tamayo P, Boehm JS, Kim SY, Moody SE, Dunn IF, et al. Systematic RNA interference reveals that oncogenic KRAS-driven cancers require TBK1. Nature 2009;462:108–12.
[13] Farshidfar F, Zheng S, Gingras MC, Newton Y, Shih J, Robertson AG, et al. Integrative genomic analysis of cholangiocarcinoma identifies distinct IDH-mutant molecular profiles. Cell Rep 2017;18:2780–94.
[14] Oishi N, Kumar MR, Roessler S, Ji J, Forgues M, Budhu A, et al. Transcriptomic profiling reveals hepatic stem-like gene signatures and interplay of miR-200c and epithelial-mesenchymal transition in intrahepatic cholangiocarcinoma. Hepatology 2012;56:1792–803.
[15] Chaisaingmongkol J, Budhu A, Dang H, Rabibhadana S, Pupacdi B, Kwon SM, et al. Common molecular subtypes among asian hepatocellular carcinoma and cholangiocarcinoma. Cancer Cell 2017;32:57–70. e3.
[16] Peraldo-Neia C, Ostano P, Cavalloni G, Pignochino Y, Sangiolo D, De Cecco L, et al. Transcriptomic analysis and mutational status of IDH1 in paired primary-recurrent intrahepatic cholangiocarcinoma. BMC Genom 2018;19:440.
[17] Jusakul A, Cutcutache I, Yong CH, Lim JQ, Huang MN, Padmanabhan N, et al. Whole-genome and epigenomic landscapes of etiologically distinct subtypes of cholangiocarcinoma. Cancer Discov 2017;7:1116–35.
[18] Ahn KS, O'Brien D, Kang YN, Mounajjed T, Kim YH, Kim TS, et al. Prognostic subclass of intrahepatic cholangiocarcinoma by integrative molecular-clinical analysis and potential targeted approach. Hepatol Int 2019;13:490–500.
[19] Miranda A, Hamilton PT, Zhang AW, Pattnaik S, Becht E, Mezheyeuski A, et al. Cancer stemness, intratumoral heterogeneity, and immune response across cancers. Proc Natl Acad Sci USA 2019;116:9020–9.
[20] Wilkerson MD, Hayes DN. ConsensusClusterPlus: a class discovery tool with confidence assessments and item tracking. Bioinformatics 2010;26:1572–3.
[21] Reich M, Liefeld T, Gould J, Lerner J, Tamayo P, Mesirov JP. GenePattern 2.0. Nat Genet 2006;38:500–1.
[22] Sia D, Hoshida Y, Villanueva A, Roayaie S, Ferrer J, Tabak B, et al. Integrative molecular analysis of intrahepatic cholangiocarcinoma reveals 2 classes that have different outcomes. Gastroenterology 2013;144:829–40.
[23] Andersen JB, Spee B, Blechacz BR, Avital I, Komuta M, Barbour A, et al. Genomic and genetic characterization of cholangiocarcinoma identifies therapeutic targets for tyrosine kinase inhibitors. Gastroenterology 2012;142:1021–31. e15.
[24] Becht E, Giraldo NA, Lacroix L, Buttard B, Elarouci N, Petitprez F, et al. Estimating the population abundance of tissue-infiltrating immune and stromal cell populations using gene expression. Genome Biol 2016;17:218.
[25] Aran D, Hu Z, Butte AJ. xCell: digitally portraying the tissue cellular heterogeneity landscape. Genome Biol 2017;18:220.
[26] Chen B, Khodadoust MS, Liu CL, Newman AM, Alizadeh AA. Profiling tumor infiltrating immune cells with CIBERSORT. Methods Mol Biol 2018;1711:243–59.
[27] Racle J, Gfeller D. EPIC: A tool to estimate the proportions of different cell types from bulk gene expression data. Methods Mol Biol 2020;2120:233–48.
[28] Plattner C, Finotello F, Rieder D. Deconvoluting tumor-infiltrating immune cells from RNA-seq data using quanTIseq. Methods Enzym 2020;636:261–85.
[29] Jiang P, Gu S, Pan D, Fu J, Sahu A, Hu X, et al. Signatures of T cell dysfunction and exclusion predict cancer immunotherapy response. Nat Med 2018;24:1550–8.
[30] Xu L, Deng C, Pang B, Zhang X, Liu W, Liao G, et al. TIP: a web server for resolving tumor immunophenotype profiling. Cancer Res 2018;78:6575–80.
[31] Liberzon A, Subramanian A, Pinchback R, Thorvaldsdóttir H, Tamayo P, Mesirov JP. Molecular signatures database (MSigDB) 3.0. Bioinformatics 2011;27:1739–40.
[32] Hänzelmann S, Castelo R, Guinney J. GSVA: gene set variation analysis for microarray and RNA-seq data. BMC Bioinforma 2013;14:7.
[33] Ritchie ME, Phipson B, Wu D, Hu Y, Law CW, Shi W, et al. limma powers differential expression analyses for RNA-sequencing and microarray studies. Nucleic Acids Res 2015;43:e47.
[34] Subramanian A, Tamayo P, Mootha VK, Mukherjee S, Ebert BL, Gillette MA, et al. Gene set enrichment analysis: a knowledge-based approach for interpreting genome-wide expression profiles. Proc Natl Acad Sci USA 2005;102:15545–50.
[35] Wu T, Hu E, Xu S, Chen M, Guo P, Dai Z, et al. clusterProfiler 4.0: a universal enrichment tool for interpreting omics data. Innovation 2021;2:100141.
[36] Chen X, Chen H, Yao H, Zhao K, Zhang Y, He D, et al. Turning up the heat on non-immunoreactive tumors: pyroptosis influences the tumor immune microenvironment in bladder cancer. Oncogene 2021;40:6381–93.
[37] Liu J, Tan Y, Zhang H, Zhang Y, Xu P, Chen J, et al. Soft fibrin gels promote selection and growth of tumorigenic cells. Nat Mater 2012;11:734–41.
[38] Leek JT, Johnson WE, Parker HS, Jaffe AE, Storey JD. The sva package for removing batch effects and other unwanted variation in high-throughput experiments. Bioinformatics 2012;28:882–3.
[39] Wang Z, Chen X, Jiang Z. Immune infiltration and a ferroptosis-related gene signature for predicting the prognosis of patients with cholangiocarcinoma. Am J Transl Res 2022;14:1204–19.
[40] Uhlén M, Fagerberg L, Hallström BM, Lindskog C, Oksvold P, Mardinoglu A, et al. Tissue-based map of the human proteome. Science 2015;347:1260419.
[41] Baker DJ, Childs BG, Durik M, Wijers ME, Sieben CJ, Zhong J, et al. Naturally occurring p16(Ink4a)-positive cells shorten healthy lifespan. Nature 2016;530:184–9.
[42] Lv Y, Wu L, Jian H, Zhang C, Lou Y, Kang Y, et al. Identification and characterization of aging/senescence-induced genes in osteosarcoma and predicting clinical prognosis. Front Immunol 2022;13:997765.
[43] Sun JX, Liu CQ, Xu JZ, An Y, Xu MY, Zhong XY, et al. A four-cell-senescence-regulator-gene prognostic index verified by genome-wide CRISPR can depict the tumor microenvironment and guide clinical treatment of bladder cancer. Front Immunol 2022;13:908068.
[44] Yu S, Chen M, Xu L, Mao E, Sun S. A senescence-based prognostic gene signature for colorectal cancer and identification of the role of SPP1-positive macrophages in tumor senescence. Front Immunol 2023;14:1175490.
[45] Lian J, Yue Y, Yu W, Zhang Y. Immunosenescence: a key player in cancer development. J Hematol Oncol 2020;13(1):151.
[46] Chibaya L, Snyder J, Ruscetti M. Senescence and the tumor-immune landscape: Implications for cancer immunotherapy. Semin Cancer Biol 2022;86(Pt 3):827–45.
[47] Peixoto E, Khan A, Lewis ZA, Contreras-Galindo R, Czaja W. The chromatin remodeler HELLS: a new regulator in dna repair, genome maintenance, and cancer. Int J Mol Sci 2022;23:9313.
[48] Sun LQ, Lee DW, Zhang Q, Xiao W, Raabe EH, Meeker A, et al. Growth retardation and premature aging phenotypes in mice with disruption of the SNF2-like gene, PASG. Genes Dev 2004;18:1035–46.